



RESEARCH LETTER

10.1002/2014GL062627

Key Points:

- Depth-averaged N governs criticality for first mode internal waves on the shelf
- Wind-mixing causes 3 day subcritical window for IT to propagate on-shelf
- Peaks in M_2 energy flux at shelf moorings are delayed relative to wind-mixing

Correspondence to:

G. R. Stephenson Jr.,
g.stephenson@bangor.ac.uk

Citation:

Stephenson, G. R., Jr., J. E. Hopkins, J. A. Mattias Green, M. E. Inall, and M. R. Palmer (2015), Baroclinic energy flux at the continental shelf edge modified by wind-mixing, *Geophys. Res. Lett.*, 42, 1826–1833, doi:10.1002/2014GL062627.

Received 24 NOV 2014

Accepted 10 FEB 2015

Accepted article online 16 FEB 2015

Published online 18 MAR 2015

This is an open access article under the terms of the Creative Commons Attribution License, which permits use, distribution and reproduction in any medium, provided the original work is properly cited.

Baroclinic energy flux at the continental shelf edge modified by wind-mixing

Gordon R. Stephenson Jr.¹, Joanne E. Hopkins², J. A. Mattias Green¹, Mark E. Inall³, and Matthew R. Palmer²

¹School of Ocean Sciences, Bangor University, Menai Bridge, UK, ²National Oceanography Centre, Liverpool, UK,

³Scottish Association of Marine Science, Oban, UK

Abstract Temperature and current measurements from two moorings onshore of the Celtic Sea shelf break, a well-known hot spot for tidal energy conversion, show the impact of passing summer storms on the baroclinic wavefield. Wind-driven vertical mixing changed stratification to permit an increased on-shelf energy transport, and baroclinic energy in the semidiurnal band appeared at the moorings 1–4 days after the storm mixed the upper 50 m of the water column. The timing of the maximum in the baroclinic energy flux is consistent with the propagation of the semidiurnal internal tide from generation sites at the shelf break to the moorings 40 km away. Also, the ~3 day duration of the peak in M_2 baroclinic energy flux at the moorings corresponds to the restratification time scale following the first storm.

1. Introduction

Where the barotropic tide flows over steep topography, internal waves are generated at tidal frequencies. Generation of this internal tide (henceforth IT) has been observed over mid-ocean ridges [e.g., Zilberman *et al.*, 2009], at island chains [e.g., Cole *et al.*, 2009], and along continental shelves [e.g., Hosegood and van Haren, 2006; Nash *et al.*, 2012]. Shelf-break-generated waves can propagate 10–100 km on-shelf [Green *et al.*, 2008; Inall *et al.*, 2011], but there is also a signal from ITs which may have been remotely generated and propagated across ocean basins onto the shelf [e.g., Nash *et al.*, 2012]. Dissipation by the breaking IT is a major sink for the global tidal energy budget [Egbert and Ray, 2001], and the associated vertical mixing may be necessary to explain the distributions of temperature and salinity in the ocean basins [Munk and Wunsch, 1998]. In shelf seas, vertically sheared currents associated with the IT impact drilling and tidal energy operations [Neill *et al.*, 2014], while mixing contributes to the vertical nutrient transport that supports productive shelf seas fisheries [e.g., Sharples *et al.*, 2007].

The IT field at a location consists of a locally generated component and a remotely generated, difficult to predict, signal with distorted phases [Nash *et al.*, 2012]. Other complications in predicting and analyzing the ITs come from mesoscale variability changing the vorticity balance along a shelf slope [Hosegood and van Haren, 2006], interference and nonlinear interaction by waves from multiple sources [e.g., Lien *et al.*, 2005; Vlasenko *et al.*, 2014], or interactions between the semidiurnal tide and near-inertial waves [Shroyer *et al.*, 2011; Hopkins *et al.*, 2014]. Hopkins *et al.* [2014] found that nonlinear interactions between wind-driven near-inertial oscillations and the internal tide alter tidal energy fluxes and produce a regular, ~2 day beat frequency in onshore and offshore fluxes. This study uses the same data set to examine a second, previously unrecognized mechanism by which the wind can affect tidal energy fluxes on short time scales, namely, how stratification changes due to wind-mixing can affect the propagation of the internal tide on the shelf. The strength of the IT is affected by seasonal stratification changes. For example, well-mixed winter conditions in the Celtic Sea, which is the area under investigation here, lack the stratification necessary to support internal waves. Shorter time scale variations in stratification, in particular those associated with wind-mixing, are also likely to impact the generation and propagation of IT from the shelf break; these effects are the focus of this study.

Freely propagating internal inertia gravity waves have frequencies $f < \omega < N$, where $f = 2\Omega \sin\phi$ ($\Omega = 7.292 \times 10^{-5} \text{ s}^{-1}$, ϕ is latitude) is the Coriolis frequency, ω is the frequency of the internal wave (here taken to be that of the semidiurnal tide), and N is the buoyancy frequency averaged over some

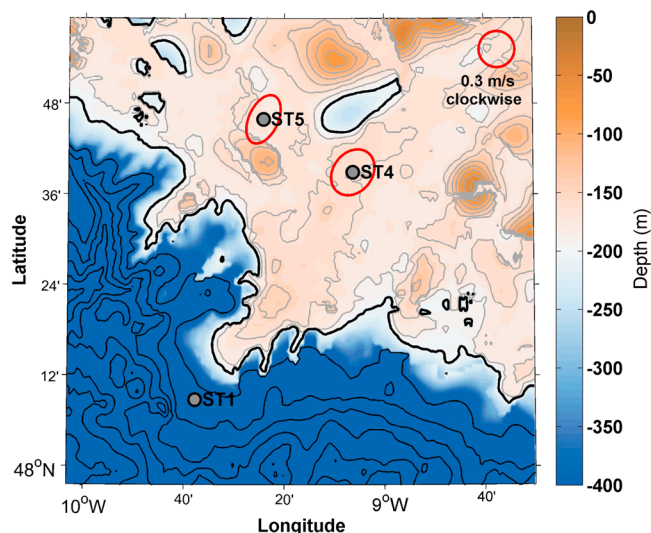


Figure 1. Bathymetry of the Celtic Sea shelf break study area with the mooring locations (gray circles). The shelf break coincides with the 200 m isobath (black line). Contour intervals are 20 m (gray) and 500 m (thin black). Water depths at the moorings are 157 m (ST4), 170 m (ST5), and 688 m (ST1). Tidal ellipses (red) are shown at ST4 and ST5, with a purely clockwise 0.3 m s^{-1} current in the corner for scale.

reflects offshore. Conversely, when $\gamma < \alpha$ the slope is subcritical and internal waves can propagate across the shelf break. Where $\gamma = \alpha$ the slope is critical and likely a hot spot of tidal conversion (IT generation) and dissipation [e.g., Lamb, 2014; Vlasenko et al., 2014].

Because the characteristic slope of an internal wave—and therefore the critical slope of topography—is dependent on the strength of the vertical stratification (see equation (2)), reducing the stratification by mixing increases the critical slope, α . For a given topographic slope, a sufficiently large change in N can therefore switch the slope from supercritical to critical or subcritical. We then expect to see a shift in generation sites as newly critical topographic slopes “switch on,” and a shift in propagation of the IT as supercritical bathymetry becomes subcritical, allowing the shoreward propagation of IT energy that would previously have been reflected. Here using observations from a mooring array deployed across the Celtic Sea shelf break in June 2012, we describe the impact of two wind-mixing events on internal wave energetics.

2. Data and Methods

As part of the June 2012 FASTNet (Fluxes across sloping topography in the northeast Atlantic) field campaign in the Celtic Sea, three moorings (ST1, ST4, and ST5) were deployed near the shelf break in an L-shaped array (see Figure 1 for details)—a configuration designed to measure across- and along-shelf energy fluxes. ST1 was deployed off-shelf, near a seaward extension of the shelf break, at 48.2°N , 9.7°W in 688 m water depth. ST4 was deployed 43 km further on-shelf at 48.7°N , 9°W in 156 m water depth. ST5 was located 26 km northwest of ST4 at 48.8°N , 9.4°W in 169 m water depth. A hill with a minimum depth of 96 m was located to the south of ST5, between the shelf break and the mooring. Smaller 10–20 m amplitude bathymetric undulations were present between ST4 and the shelf break (Figure 1). For the calculations of bathymetric slope, we used a 1/120 degree resolution, gridded General Bathymetric Chart of the Oceans (GEBCO_08, available from <http://www.gebco.net/>).

The moorings were fitted with Star-Oddi mini temperature loggers spaced 2–20 m apart with the smaller spacing across the thermocline, MicroCATs to measure conductivity and temperature, and bottom-mounted Acoustic Doppler Current Profilers (ADCPs). Temperature and conductivity were recorded once per minute. A Flowquest 150 kHz ADCP at ST4 returned current ensembles at 1 min intervals in 2 m vertical bins from ~ 8 m to 145 m above the bottom with the last bin ~ 11 m below the surface. At ST5, an RDI 150 kHz ADCP with 2 min sampling intervals and 2.5 m vertical bins measured from ~ 8 m above the bottom to ~ 21 m below the surface. Full details of the instrumentation and data processing are described in Hopkins et al. [2014]

suitable depth range defined by

$$N^2 = -\frac{g}{\rho_0} \frac{d\rho}{dz}, \quad (1)$$

where ρ is in situ density, ρ_0 is a representative average density, and z is height. The energy of an internal wave propagates along a characteristic raypath with a slope α relative to the horizontal, defined by

$$\alpha^2 = \frac{\omega^2 - f^2}{N^2 - \omega^2}. \quad (2)$$

Equation (2) also defines a critical topographic slope. Where internal waves encounter topography, they generally reflect off the bottom, potentially with a small amount of dissipation taking place [Lamb, 2014], but if the slope of the seabed, γ , is greater than α , i.e., if the slope is supercritical, propagation of the internal wave in the upslope direction is not permitted, and the wave energy

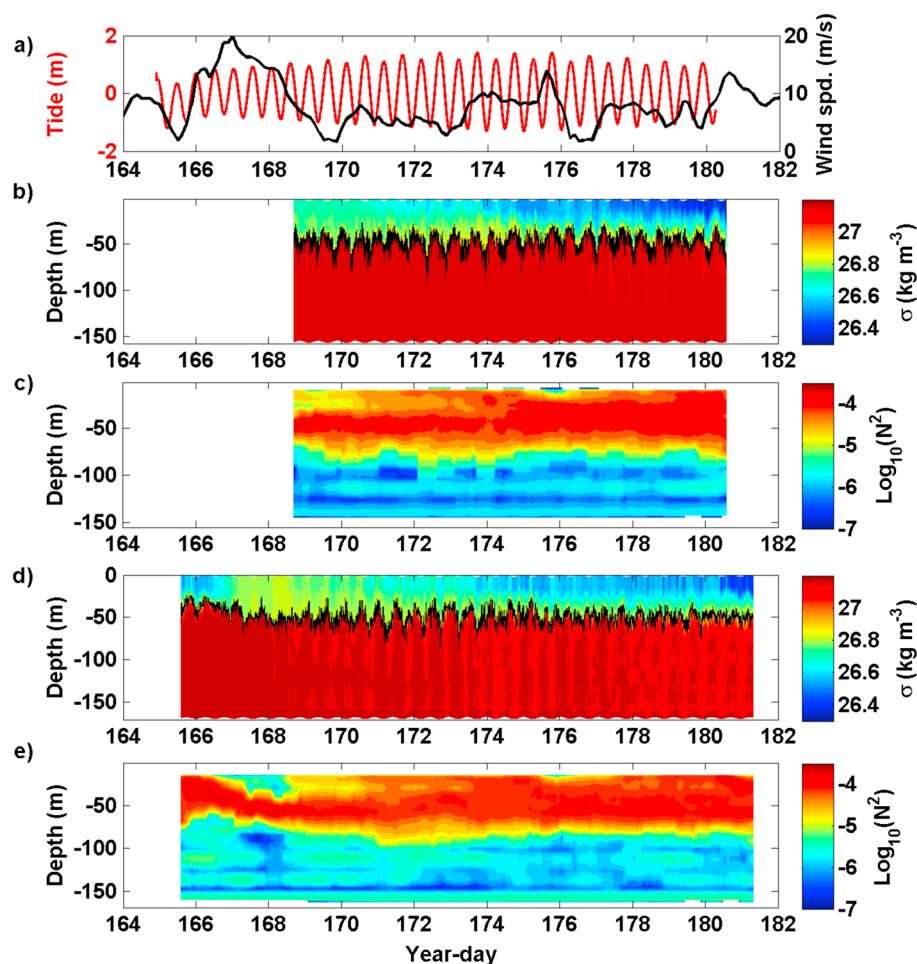


Figure 2. (a) Tidal displacement at ST1 (red) and ECMWF ERA wind speed (black) at 48.75°N, 9.75°W. (b) Potential density and (c) N^2 at ST4. (d) Potential density and (e) N^2 at ST5. In Figures 2b and 2d, the black line indicates the depth of the 1026.9 kg m⁻³ isopycnal.

and Vlasenko *et al.* [2014]. The data were used to calculate M_2 baroclinic energy fluxes from the correlation between semidiurnal perturbations in velocity and pressure (see, e.g., Kunze *et al.* [2002] for details). Power spectra of the baroclinic currents [see Hopkins *et al.*, 2014, Figure 4] show distinct, well-separated peaks at inertial and M_2 tidal frequencies, so in computing the M_2 energy fluxes, a 58 h window was used, sufficient to resolve the difference between inertial (~ 16 h period) and M_2 (12.4 h period) signals.

Gridded wind fields from the European Centre for Medium-Range Weather Forecasting (ECMWF) Extended-Range Re-Analysis (ERA) Interim product show that strong winds (>15 m s⁻¹) were present over the mooring sites on year-days 166–169 and 175 (Figure 2a; data from http://badc.nerc.ac.uk/view/badc.nerc.ac.uk__ATOM_datent__12458543158227759). The first gale delayed the deployment of ST4, but ST1 and ST5 captured the wind-mixing. During the first gale (days 166–169), the upper ocean at ST5 cooled by 1.1°C and the mixed layer deepened from 40 m to 60 m depth (Figure 2d). There followed a gradual warming and restratification of the surface layer during the following days, until the second gale on days 175–176.

3. Stratification Changes and Critical Slopes

The criticality of ocean bathymetry relative to an internal wave depends on the ratio between the characteristic slope of the internal wave and the slope of the bathymetry. The calculation of criticality is therefore sensitive to the vertical scale over which N is averaged. Common practice has been to use the buoyancy frequency measured near or just above the seabed (N_{bot}) to determine the critical topographic

slope [Llewellyn Smith and Young, 2002; Nycander, 2005]. This approach is based on a WKB approximation to internal wave solutions, which assumes that topographic slopes are much smaller than the slopes of tidal beams and that the topographic height is much less than the vertical wavelength of the internal tide. In the relatively shallow shelf sea under study here, isopycnal displacements of 50 m are not uncommon nor are these small relative to the ~ 200 m water depth (Figures 2b and 2d). A recent study of tidal conversion rates by Zarroug *et al.* [2009] suggests that the WKB approach using N_{bot} underestimates conversion rates for the gravest modes of the internal tide. Instead, averaging buoyancy frequency over the vertical wavelength of the internal wave yields more accurate tidal conversion rates. For the first baroclinic mode, this is equivalent to averaging N over the depth of the water column. Although our study does not calculate conversion rates, this approach is suited to our exploration of the interactions between the internal tide and topography.

An important point to note is that the appropriate stratification to consider for topographic criticality of the mode 1 internal tide is the depth average of N rather than of N^2 . Depth-averaged N^2 , $\langle N^2 \rangle$, is determined solely by the surface-to-bottom buoyancy difference, independent of the water column structure. This is not true of the depth-averaged N , $\langle N \rangle$. In uniformly stratified water, $\langle N \rangle = \sqrt{\langle N^2 \rangle}$, but for any nonuniform stratification profile, $\langle N \rangle < \sqrt{\langle N^2 \rangle}$. If N_{crit} represents the critical value of stratification for a given topographic slope, $\sqrt{\langle N^2 \rangle} < N_{\text{crit}}$ is sufficient to infer that the slope is subcritical, since $\langle N \rangle < \sqrt{\langle N^2 \rangle}$, but $\sqrt{\langle N^2 \rangle} > N_{\text{crit}}$ does not prove that a slope is supercritical. Consider the simple case of a water column of depth H with $N(z) = N_1$ everywhere except in a pycnocline of thickness h , where $N(z) = N_2$. Fixing $\langle N^2 \rangle = \frac{1}{H} ((H-h)N_1^2 + hN_2^2)$ constant, we rearrange to find $N_2 = \sqrt{\frac{h}{H}\langle N^2 \rangle - \frac{H-h}{h}N_1^2}$, which yields

$$\langle N \rangle = \left(1 - \frac{h}{H}\right) N_1 + \sqrt{\frac{h}{H} \sqrt{\langle N^2 \rangle} - \left(1 - \frac{h}{H}\right) N_1^2}. \quad (3)$$

In the limit $N_1 \rightarrow 0$, $\langle N \rangle \approx \sqrt{\frac{h}{H} \sqrt{\langle N^2 \rangle}}$; a sharpening of the pycnocline reduces $\langle N \rangle$ and increases the characteristic wave slope (equation (2)). In the limit of a two-layer wave with a discrete density step at the interface, $N_1 \rightarrow 0$, $h \rightarrow 0$, and $\langle N \rangle \rightarrow 0$. This implies that there is no critical bathymetric slope for a two-layer wave, consistent with two-layer wave dynamics.

To determine the characteristic slope of the M_2 IT, and hence the critical topographic slope, we calculated $\langle N \rangle$. We extended our N profiles over the whole depth of the water column by assuming N is constant in the depth intervals nearest the surface and seabed. Wind-mixing in response to the storms on days 168 and 175 decreases the stratification near the surface (Figures 2b and 2d) and, consequently, the depth-averaged stratification (Figure 3a). The buoyancy frequency at the bed, N_{bot} , is roughly half the depth-averaged stratification (Figure 3a). At ST5, $\langle N \rangle$ decreases from an initial value of $4.8 \times 10^{-3} \text{ s}^{-1}$ on year-day 166 to $3.0 \times 10^{-3} \text{ s}^{-1}$ on year-day 168 (Figure 3b). Restratification follows the reduction in wind speed; $\langle N \rangle$ increases to $4.8 \times 10^{-3} \text{ s}^{-1}$ by year-day 172. However, the wind event on day 176 is followed by a slight decrease in stratification. ST4 shows a similar restratification to ST5 (Figure 3a). Figure 3a also shows the average stratification in the upper 200 m at ST1, to represent how conditions might vary south and west of ST4 and ST5, nearer the shelf break. The decreases in $\langle N \rangle$ on day 175 are larger at ST1 and ST5 than at ST4, most likely due to spatial variability in the wind field. Conditions over the shelf were likely intermediate between the values at ST1 and those at ST4 and ST5.

The slope of critical topography is estimated according to equation (2), using measured values of $\langle N \rangle$, with $\omega = 1.4 \times 10^{-4} \text{ s}^{-1}$ (i.e., for the semidiurnal M_2 tide) and $f = 1.1 \times 10^{-4} \text{ s}^{-1}$. For the range of stratification observed at the moorings ($\langle N \rangle = 2.9 - 5.8 \times 10^{-3} \text{ s}^{-1}$), potentially critical topographic slopes are between 0.015 and 0.030 (Figure 3b). Topographic slope ranges from 10^{-3} to 10^{-1} over the Celtic Sea shelf break (Figure 4a). Figure 4a shows distribution functions of the maximum topographic slope along a ray directed from the shelf break to ST4 and ST5 for varying angles ranging from 148° to 328° , measured clockwise from north (i.e., from the “off-shelf” direction defined in Hopkins *et al.* [2014]). The proximity of the rise south of ST5 makes those slopes generally larger for ST5 than ST4. We suggest that topographic slopes between 0.015 and 0.030 are supercritical at the start of the experiment—before the wind-mixing event—and reflect IT wave energy back toward the open ocean. As stratification is reduced, these slopes become subcritical and allow M_2 energy to propagate onto the shelf. Figure 4 illustrates the criticality parameter (α/γ) for $\alpha = 0.015$ (Figure 4b) and $\alpha = 0.030$ (Figure 4c). After mixing, there are fewer areas of critical topography on the shelf, and fewer obstacles in the path of an internal wave from the shelf break to the moorings.

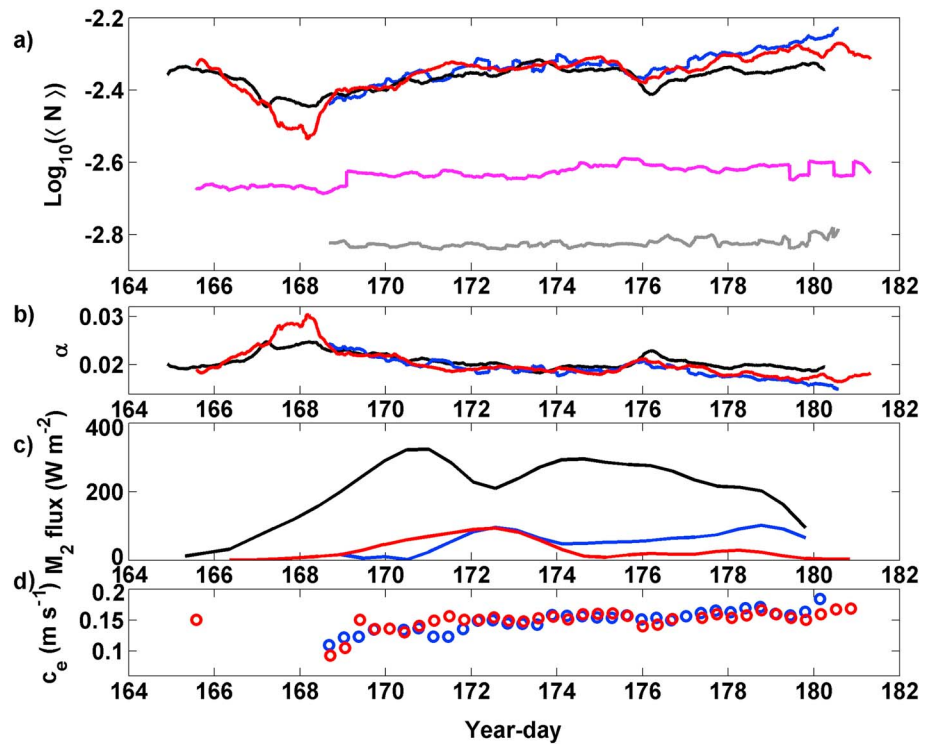


Figure 3. (a) Depth-averaged stratification ($\langle N \rangle$) at ST4 (blue) and ST5 (red). Average stratification in the top 200 m at ST1 is shown in black. We assumed constant stratification above the shallowest measurement and below the deepest measurement. Near-bed stratification is represented by the deepest value of N at ST4 (gray) and ST5 (magenta). (b) Characteristic slope of the M_2 internal tide for the values of $\langle N \rangle$ in Figure 3a at ST1 (black), ST4 (blue), and ST5 (red). (c) Magnitude of the M_2 energy flux at ST1 (black), ST4 (blue), and ST5 (red) calculated by Hopkins *et al.* [2014]. (d) Modal speed of the first baroclinic mode calculated for N^2 profile at ST4 (blue) and ST5 (red). Missing values occur when values of $N(z)$ were less than f .

4. Propagation of M_2 Internal Waves at ST4 and ST5

The response of the IT to the wind events is evident in changes in the strength of baroclinic energy fluxes at the moorings following the wind-mixing. The magnitude of the M_2 energy fluxes at the on-shelf moorings is very low at the start of the experiment but increases following the storm until a maximum of $\sim 100 \text{ W m}^{-2}$ is reached on year-day 172.6 (Figure 3c) at both ST4 and ST5. At the shelf slope mooring, ST1, a local minimum in M_2 baroclinic energy flux occurs on the same day (Figure 3c). The flux magnitude at ST1 appears to decrease by $\sim 100 \text{ W m}^{-1}$ from year-day 171 to 172.6, seemingly balancing out the increase seen at ST4 and ST5. Note, however, that ST1 may very well be located within the generation zone of the IT, which may lead to biased results [e.g., Green *et al.*, 2008]. Nonetheless, Figure 3c shows that during days 171–174 there was a decrease in M_2 energy on the shelf slope and an increase in M_2 energy on the shelf, suggesting a change in propagation of the IT following the storm. This is further supported by the fact that the decrease in energy during days 173–174 at ST4 and ST5 takes place at spring tides, i.e., during a period when we would expect to see an increase in the energy flux. A small increase in M_2 energy flux is seen at ST5 on day 178, and M_2 energy flux of $\sim 100 \text{ W m}^{-2}$ is evident on day 179 at ST4. Bathymetry has gentler slopes, in general, between ST4 and the shelf break (Figure 4a) than between ST5 and the shelf break; therefore, the smaller reduction in stratification during the second wind event on days 175–176 results in a larger increase in the internal tide energy reaching ST4.

While the decrease in energy flux from days 173 to 174 coincides with a period of restratification, the peaks in M_2 baroclinic energy fluxes on days 172–173 and 178–179 are delayed by a few days (~ 4 days and ~ 3 days, respectively) relative to the minima in stratifications on days 168 and 176. These delays may reflect the time required for energy to propagate from internal tide generation sites near the shelf break to the moorings. We estimate the propagation speed of the internal tide by numerically solving the standard eigenvalue problem of linear internal wave theory [e.g., MacKinnon and Gregg, 2003], solving for the

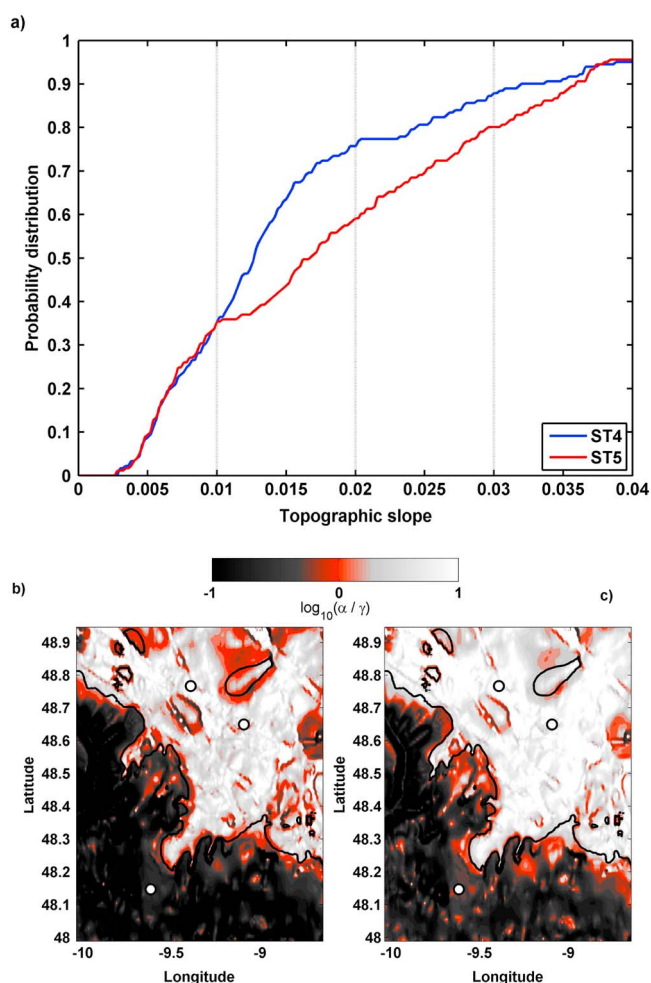


Figure 4. (a) Distribution function of the maximum topographic slopes between the 200 m isobath and moorings ST4 (blue) and ST5 (red) for paths approaching each mooring from an offshore direction. \log_{10} of the criticality parameter (α/γ) for (b) stratified ($\alpha = 0.015$) and (c) mixed ($\alpha = 0.030$) conditions.

propagation of the M_2 IT from generation sites at the shelf break to moorings ~ 40 km away. The ~ 3 day duration of the peak in M_2 baroclinic energy at the moorings matches the time required for the upper water column to restratify following the initial storm.

What caused the increase in M_2 energy at the on-shelf moorings at ST4 and ST5? The increase could be explained by increased IT generation at the shelf break. However, the stratification is shown to decrease during the storm, which would lead to a decreased tidal conversion rate [e.g., Baines, 1982]. What we see must therefore be a redistribution of the baroclinic energy. A shift in the location of tidal generation toward ST4 and ST5 and away from ST1 would accomplish this redistribution; being closer to the generation site would allow for less dissipation and more energy reaching ST4 and ST5, while less energy would reach a more distant ST1. This situation also seems unlikely: reduced stratification implies a steeper critical slope, and steeper topographic slopes are generally found farther off-shelf, toward ST1 and away from ST4 and ST5. Storm-induced changes in internal wave reflection would also redistribute baroclinic energy. We conclude that a reduction in stratification over the shelf region changed the criticality of topography between the shelf break and moorings from supercritical to subcritical. During a well-mixed “subcritical window” the M_2 IT was able to propagate on-shelf, over previously supercritical topographic slopes. Following restratification, these slopes became supercritical again and resumed reflecting incoming M_2 baroclinic energy.

dynamical modes using a routine by Klinck [1999]. Based on profiles of N^2 at ST4 and ST5 (Figures 2c and 2e), the speed of the first baroclinic mode ranges from 0.12 m s^{-1} shortly after the first storm to 0.18 m s^{-1} toward the end of the record. At these speeds, a wave travels ~ 10 to 15 km per day, so an M_2 internal wave generated at the point on the shelf break nearest ST5 during the stratification minimum on year-day 168 would appear at ST5 around day 172. Our observations show that the M_2 baroclinic energy flux at ST5 begins increasing on day 169 but peaks at day 172. The proximity of ST5 to the potentially subcritical topography may explain why the increase in M_2 energy flux is seen earlier at ST5 than at ST4. The duration of the energy flux maximum at ST4 and minimum at ST1 is ~ 3.3 days (Figure 3c), similar to the 3.6 days duration of the near-surface minimum in stratification at ST5 (Figure 3e).

5. Discussion

Baroclinic energy at the semidiurnal tidal frequency appears at moorings on the Celtic Sea continental shelf 1–4 days after a strong wind event thoroughly mixed the upper 50 m of the water column. The timing of the maximum in M_2 frequency baroclinic energy is consistent with the propa-

Our assumption that stratification at ST5 is representative of stratification over most of the shelf is useful. If wind-mixing affects stratification no deeper than 100 m, the effect of wind-mixing on stratification is reduced in deeper water; stratification changes at ST1 are smaller than those at ST4 and ST5. However, the depth at ST5 is 170 m, compared with ~200 m near the shelf break, where we posit the IT generation sites, and 157 m at ST4, so the error on our estimates of critical topographic slopes resulting from depth variations is only ~20%. Qualitatively, the story is robust; with our approximation, the critical topographic slope increased by a factor of 2. Small errors in the critical topographic slope will affect only slightly the timing and duration of the subcritical window for the relevant topography. Here we have used a depth-average stratification, $\langle N \rangle$, rather than the near-bed stratification, an approach which has been shown to be more accurate for the first baroclinic mode [Zarroug *et al.*, 2009]. Future studies on how the vertical structure of N controls internal wave reflection are required to confirm our hypothesis that $\langle N \rangle$ is sufficient for the first baroclinic mode and to extend our results to higher modes.

In summary, our results demonstrate the potential of time-varying stratification to drastically alter the propagation of internal waves across the continental shelf. The proposed mechanism of changes in criticality at the shelf break and on the shelf is a potential source of temporal variability in the IT. We observed variability with a time scale of a few days, but our results may be more broadly applicable to changes in shelf sea stratification on, for example, seasonal time scales. Changes in the internal tide propagation affect where the IT breaks and, consequently, the location of energy dissipation and mixing in shelf seas. This is crucially important to estimates of the vertical nutrient transport that supports shelf seas fisheries. Near-critical slopes are ubiquitous in the ocean and global tidal energy budgets or tidal models would therefore benefit from consideration of time-varying stratification. We conjecture that this mechanism may also be relevant to waters not directly mixed by the wind. Where a topographic slope is close to sea ice or sheltered areas (e.g., a fjord), a supercritical/subcritical switch induced by wind-mixing over a near-critical slope may allow IT energy to propagate into normally sheltered water.

Acknowledgments

Funding was provided through the National Environmental Research Council through the FASTNET consortium (NE/I030224/1) and an Advanced Fellowship (NE/F014821/1, awarded to J.A.M.G.). The expertise of the crew of RV *Discovery*, Cruise D376, is gratefully acknowledged, especially the assistance by Colin Griffiths, Estelle Dumont, and Terry Doyle. Insightful feedback from three anonymous reviewers has honed our scientific ideas and greatly improved this manuscript. The GEBCO Digital Atlas is published by the British Oceanographic Data Centre on behalf of IOC and IHO, 2003. The data used are available from the British Oceanographic Data Center (<http://www.bodc.ac.uk/>).

The Editor thanks two anonymous reviewers for their assistance in evaluating this paper.

References

- Baines, P. G. (1982), On internal tide generation models, *Deep Sea Res., Part A*, 29(3A), 307–338.
- Cole, S. T., D. L. Rudnick, B. A. Hodges, and J. P. Martin (2009), Observations of internal wave beams at Kauai Channel, Hawaii, *J. Phys. Oceanogr.*, 39, 421–436, doi:10.1175/2008JPO3937.1.
- Egbert, G. D., and R. D. Ray (2001), Estimates of M_2 tidal energy dissipation from TOPEX/Poseidon altimeter data, *J. Geophys. Res.*, 106, 22,475–22,502, doi:10.1029/2000JC000699.
- Green, J. A. M., J. H. Simpson, S. Legg, and M. R. Palmer (2008), Internal waves, baroclinic energy fluxes, and mixing at the European shelf edge, *Cont. Shelf Res.*, 28, 937–950, doi:10.1016/j.csr.2008.01.014.
- Hopkins, J. E., G. R. Stephenson, J. M. Green, M. E. Inall, and M. R. Palmer (2014), Storms modify baroclinic energy fluxes in a seasonally stratified shelf sea: Inertial-tidal interaction, *J. Geophys. Res. Oceans*, 119, 6863–6883, doi:10.1002/2014JC010011.
- Hosegood, P., and H. van Haren (2006), Sub-inertial modulation of semi-diurnal currents over the continental slope in the Faeroe-Shetland Channel, *Deep Sea Res., Part I*, 53, 627–655, doi:10.1016/j.dsr.2005.12.016.
- Inall, M., D. Aleynik, T. Boyd, M. Palmer, and J. Sharples (2011), Internal tide coherence and decay over a wide shelf sea, *Geophys. Res. Lett.*, 38, L23607, doi:10.1029/2011GL049943.
- Klinck, J. (1999), *Dynmodes.m—Ocean Dynamic Vertical Modes*, Woods Hole Science Center - SEA-MAT - Matlab Tools for Oceanographic Analysis, Woods Hole, Mass. [Available at <http://woodshole.er.usgs.gov/operations/sea-mat/index.html>, Accessed 2014-August-13.]
- Kunze, E., L. Rosenfeld, G. Carter, and M. Gregg (2002), Internal waves in Monterey submarine canyon, *J. Phys. Oceanogr.*, 32, 1890–1913.
- Lamb, K. G. (2014), Internal wave breaking and dissipation mechanisms on the continental slope/shelf, *Annu. Rev. Fluid Mech.*, 46, 231–254, doi:10.1146/annurev-fluid-011212-140701.
- Lien, R.-C., T. Y. Tang, M. H. Chang, and E. A. d'Asaro (2005), Energy of nonlinear internal waves in the South China Sea, *Geophys. Res. Lett.*, 32, L05615, doi:10.1029/2004GL022012.
- Llewellyn Smith, S. G., and W. R. Young (2002), Conversion of the barotropic tide, *J. Phys. Oceanogr.*, 32, 1554–1566.
- MacKinnon, J. A., and M. C. Gregg (2003), Shear and baroclinic energy fluxes on the summer New England shelf, *J. Phys. Oceanogr.*, 33, 1462–1475, doi:10.1175/1520-0485(2003)033<1462:SABEFO>2.0.CO;2.
- Munk, W., and C. Wunsch (1998), Abyssal recipes II: Energetics of tidal and wind mixing, *Deep Sea Res., Part I*, 45, 1977–2010.
- Nash, J. D., S. M. Kelly, E. L. Shroyer, J. N. Moum, and T. F. Duda (2012), The unpredictable nature of internal tides on continental shelves, *J. Phys. Oceanogr.*, 42, 1981–2000, doi:10.1175/JPO-D-12-028.1.
- Neill, S. P., M. R. Hashemi, and M. J. Lewis (2014), The role of tidal asymmetry in characterizing the tidal energy resource of Orkney, *Renewable Energy*, 68, 337–350, doi:10.1016/j.renene.2014.01.052.
- Nycander, J. (2005), Generation of internal waves in the deep ocean by tides, *J. Geophys. Res.*, 110, C10028, doi:10.1029/2004JC002487.
- Sharples, J., *et al.* (2007), Spring-neap modulation of internal tide mixing and vertical nitrate fluxes at a shelf edge in summer, *Limnol. Oceanogr.*, 52, 1735–1747.
- Shroyer, E. L., J. N. Moum, and J. D. Nash (2011), Nonlinear internal waves over New Jersey's continental shelf, *J. Geophys. Res.*, 116, C03022, doi:10.1029/2010JC006332.

- Vlasenko, V., N. Stashchuk, M. Inall, and J. E. Hopkins (2014), Tidal energy conversion in a global hotspot: On the 3-D dynamics of baroclinic tides at the Celtic Sea shelf break, *J. Geophys. Res. Oceans*, *119*, 3249–3265, doi:10.1002/2013JC009708.
- Zarroug, M., J. Nycander, and K. Döös (2009), Energetics of tidally generated internal waves for nonuniform stratification, *Tellus*, *62A*, 71–79, doi:10.1111/j.1600-0870.2009.00415.x.
- Zilberman, N. V., J. M. Becker, M. A. Merrifield, and G. S. Carter (2009), Model estimates of M_2 internal tide generation over Mid-Atlantic Ridge topography, *J. Phys. Oceanogr.*, *39*, 2635–2651, doi:10.1175/2008JPO4136.1.